Investigation of the Noise Effect on Tomographic Reconstructions for a Tangentially Viewing Vacuum Ultraviolet Imaging Diagnostic*)

Tingfeng MING[1)], Satoshi OHDACHI[1,2)], Yasuhiro SUZUKI[1,2)] and LHD Experiment Group[2)]

[1)]*The Graduate University for Advanced Studies, Toki 509-5292, Japan*

[2)]*National Institute for Fusion Science, Toki 509-5292, Japan*

(Received 20 December 2010 / Accepted 3 June 2011)

Tomographic reconstruction for a tangentially viewing two-dimensional (2D) imaging system is studied. A method to calculate the geometry matrix in 2D tomography is introduced. An algorithm based on a Phillips-Tikhonov (P-T) type regularization method is investigated, and numerical tests using the P-T method are conducted with both tokamak and Heliotron configurations. The numerical tests show that the P-T method is not sensitive to the added noise levels and the emission profiles with higher mode numbers can be reconstructed with adequate resolution. The results indicate that this method is suitable for 2D tomographic reconstruction for a tangentially viewing vacuum ultraviolet telescope system.

Keywords: tomography, reconstruction, VUV, GCV, LHD

DOI: 10.1585/pfr.6.2406120

1. Introduction

In magnetic confined plasma, the MHD activities play an important role in confinement. A complete understanding of the MHD fluctuations is necessary for obtaining stable operation with good confinement. Although the predictions of the threshold values of the plasma parameters for the appearance of MHD instabilities are in good agreement with the experimental data, their evolutions and the relationship between the MHD activities and transport is not clear. A two-dimensional (2D) imaging system may be helpful in investigating the fluctuations and their typical characteristics because the 2D structure of the fluctuations can be obtained with temporal and spatial resolution by using this diagnostics.

A tomographic reconstruction technique has been used to evaluate the local emission profile from line-integrated measurements obtained using multi-channel detectors in fusion plasmas. In the current fusion plasma research, 2D detectors, e.g., CCD cameras, have been widely used as powerful diagnostic tools [1, 2] because they provide two advantages over conventional diagnostic arrays: (1) much larger number of viewing lines and (2) the viewing lines can measure the emission from different planes, e.g., poloidal cross sections in different toroidal positions.

To investigate the fluctuations, especially the ones that are localized in the edge plasma, a 2D VUV telescope system has been developed in the Large Helical Device (LHD) [3]. The telescope was transferred from a perpendicular port to a tangential port during the 2010 campaign. Photons of 13.5 nm can be detected by this diagnostic system. Emissions from CVI (n = 4 to n = 2 transition) near 13.5 nm can be measured and is obtained from the emission integral along the viewing lines. In general, the intensity of the emission is proportional to the local electron and impurity densities. The density fluctuations can be estimated using the VUV camera system. For studying the 2D emission profile at a poloidal cross section, it is desired to develop a suitable tomographic algorithm.

The VUV emission is localized at the very edge of the parameter range; investigating the applicability and performance of the tomographic reconstruction when the emission is localized in this edge region is important.

In this paper, the algorithm used for the tomographic reconstruction is briefly introduced in section 2. The method for generating the geometry matrix is described in section 3. Numerical tests with the tokamak and LHD configurations are shown in section 4.

2. Algorithm for Tomography

For a 2D emission profile $E(x, y)$, the ith nonlocal measurement can be described by

$$I_i = \iint S_i(x, y)E(x, y)\mathrm{d}x\mathrm{d}y. \qquad (1)$$

After the pixelation of image E with j grids, the discrete linear algebra form of (1) is obtained:

$$\boldsymbol{I} = \mathsf{S}\boldsymbol{E}, \qquad (2)$$

where S is the so-called geometry matrix, in which each

author's e-mail: ming_tingfeng@LHD.nifs.ac.jp

*) This article is based on the presentation at the 20th International Toki Conference (ITC20).

component S_{ij} describes the contribution from the ith viewing line due to the emission at grid j. $\boldsymbol{E}$ is the image vector and $\boldsymbol{I}$ is the line-integrated measured data. The function of tomography is to solve Eq. (2) for a given $\boldsymbol{I}$; however, it is an ill-posed problem [4]. Because there are many solutions satisfying equation (2), regularization of the solutions according to specific requirements such as smoothness of the emission profile is required.

It is equivalent to the minimization of the quantity J:

$$J \equiv \gamma P(E) + \frac{1}{M}\|\mathsf{S}\boldsymbol{E} - \boldsymbol{I}\|^2, \tag{3}$$

where γ is the regularization parameter; it controls the degree of smoothness of the solution. To select the optimum regularization parameter, a minimization of the generalized cross validation (GCV) is used [5]. The GCV is defined as follows:

$$V(\gamma) = M\|(\mathsf{I}_M - \mathsf{A}(\gamma))\boldsymbol{I}\|^2/\{\mathrm{Trace}(\mathsf{I}_M - \mathsf{A}(\gamma))\}^2, \tag{4}$$

where, I_M denotes the $M \times M$ unit matrix, and $\mathsf{A}(\gamma) = \mathsf{S}(\mathsf{S}^T\mathsf{S} + M\gamma\mathsf{C}^T\mathsf{C})^{-1}\mathsf{S}^T$. Here, $P(E)$ is an introduced penalty function and M is the total number of viewing lines.

Several algorithms have been developed to perform this regularization. In the Phillips-Tikhonov (P-T) type method proposed in [4], a penalty function is defined in the linear form of

$$P(E) = \|\mathsf{C}\boldsymbol{E}\|^2\,, \tag{5}$$

where C is a laplacian operator. Therefore, the solution is given under the constraint of a minimization of the mean-squared error and laplacian $\nabla^2 E(x, y)$ on the image. In this study, reconstructions are performed using the P-T method.

A parameter d^2 is selected to show the quality of reconstruction, which is defined as follows:

$$d^2 = \frac{1}{J}\sum_j (E_j - E_j^*)^2/E_{\max}^2, \tag{6}$$

where, J is the total number of grids, E_j, E_j^*, and $E_{\max}$ are the jth reconstructed value, assumed value, and the peak value of the assumed profile, respectively.

3. Calculation of the Geometry Matrix

Before performing the tomographic reconstruction, the geometry matrix should be determined with high accuracy. For real measurements, the signals are obtained along strips with a finite width. Here, the integral in the strips is approximated by the line integrals along the viewing lines. Under this assumption, the calculation of the geometry matrix is relatively easy.

There are many reports suggesting that the emission profile is reconstructed with good accuracy only if the plasma is observed from various directions [6].

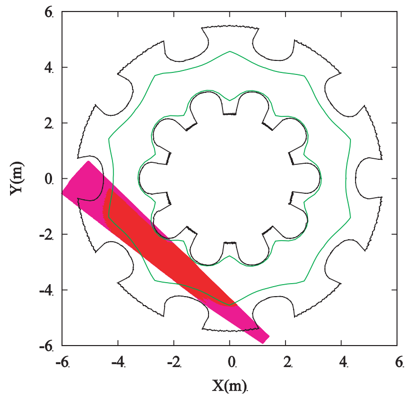

Fig. 1 The viewing field of the tangentially viewing telescope system in LHD.

In 2D detector systems, only one camera is usually used; therefore, if we assume arbitrary 3D emission profiles, reconstructions cannot be performed. Here, an assumption of constant radiation along the magnetic field line is made [7]. Thereby, a 2D emission profile is assumed.

To construct the geometry matrix, a viewing line is projected to a curved line on a poloidal target plane Pt. The line elements in a viewing line are connected to the elements in the curved line with magnetic field lines as described in [7]. In the calculation of the VUV camera geometry in the LHD, the magnetic field is estimated by the equilibrium code HINT-2 [8, 9] here, because we expect VUV emission from the boundary of the LHD plasma and, the magnetic field lines, which are outside the last closed flux surface, can be estimated by HINT-2. An example of the 2D camera geometry is shown in Fig. 1. This is the arrangement of the VUV camera system in the LHD. The pink area indicates the viewing field of the tangentially viewing VUV telescope and the red area is the effective viewing area. The green solid lines represent the inner and outer plasma edge (LCFS) at the equatorial plane. And the black solid lines indicate the LHD wall. In the calculation of the geometry matrix, small triangle elements are used to simulate the LHD wall. The calculation for a sight line will be ceased once the first point of intersection between the sight line and the triangle elements is found. Then, only the effective elements are recorded as one element in the matrix (Fig. 1). Figure 2 illustrates the viewing line projections on a horizontally elongated cross section, which is calculated using an equilibrium with the averaged-beta $\beta \sim 1.4\%$ and the preset magnetic axis $R_{\mathrm{ax}} = 3.75$ m. The green curves indicate the magnetic surfaces and the red lines are part of the sight line projections. The target plane Pt is divided into grids, and then the number of elements in the ith viewing line inside the jth grid is counted. The geometry matrix can be constructed from this number.

Note that the entire area is not covered equally; in the upper region, the coverage is much denser compared with

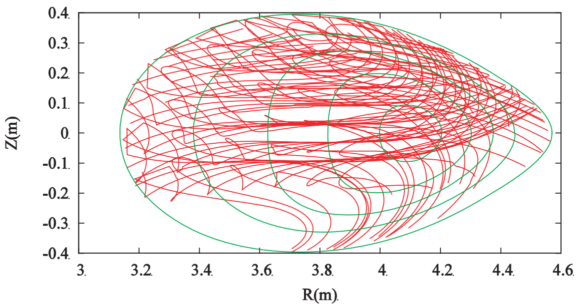

Fig. 2 Projections of viewing lines on the plane Pt. A configuration of LHD plasma with vacuum magnetic axis $R_{ax} = 3.75$ m, $<\beta> = 1.4\%$.

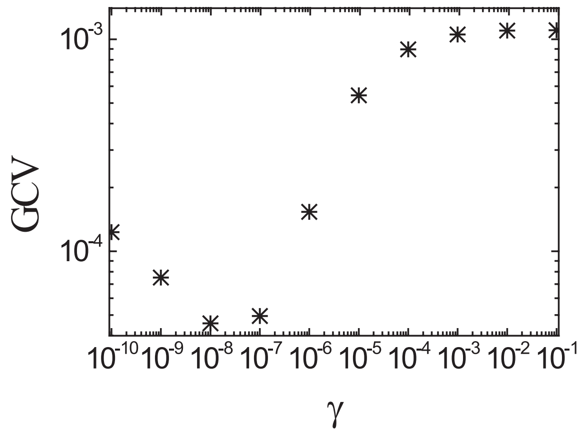

Fig. 3 GCV obtained in the reconstruction. The minimum GCV indicates an optimized regularization parameter.

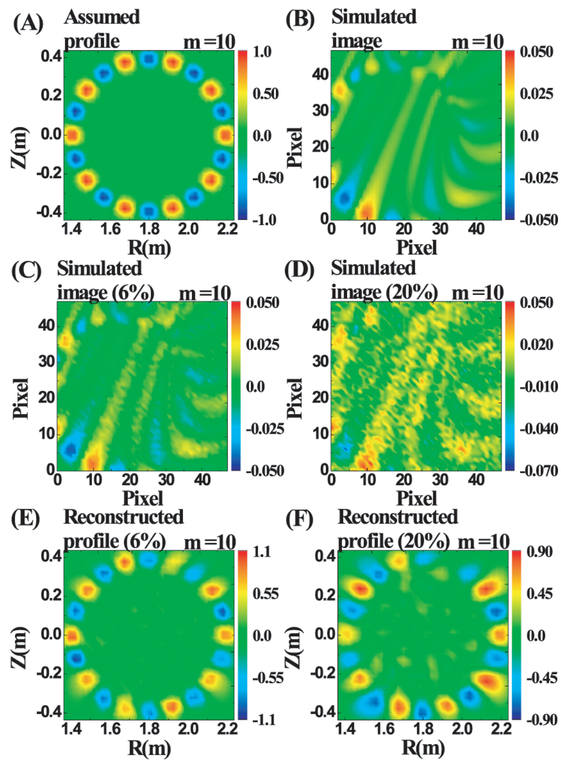

Fig. 4 Tests for an assumed profile with $m = 10$: (A) assumed profile, (B) line-integrated image; (C) and (D) are simulated images with 6% and 20% normally distributed added noise, respectively; (E) and (F) are reconstructed profiles of (C) and (D), respectively.

that in the lower region. In the dense areas, several viewing lines from various viewing angles pass through one pixel, whereas in the sparse areas, most viewing lines are parallel in a single pixel. In the lower left part of Fig. 2, the space area (no coverage of viewing line) is due to the arrangement of the VUV camera, resulting in the lack of viewing lines in the outer part of LHD chamber, as shown in Fig. 1.

4. Numerical Tests

To examine the capability of the tomography method, we perform a so-called phantom simulation. In phantom simulations, synthetic line-integrated data are calculated with the geometry matrix and the assumed emission profile; then, a realistic level of random noise is added, and the reconstruction of the local emission profile is examined.

The GCV method is adopted to select the optimum regularization parameter. The reconstructions by the P-T method show a clear minimized GCV, which indicates that an optimum regularization parameter can be determined. Figure 3 shows GCV as a function of the regularization parameter at a high mode number ($m = 10$) reconstruction of the tokamak configuration, where 6% noise is added to the line-integrated data [Fig. 4 (E)]. The results shown are obtained with an optimized regularization parameter.

4.1 Numerical tests with tokamak configuration

To check the efficiency of the algorithms for the 2D reconstruction of the edge localized emissions, e.g., VUV light, the emission profile is assumed to be localized in the edge region ($\rho \sim 0.9$). The reconstructions of profiles with high mode numbers have been investigated using the tokamak configuration. In these tests, a TEXTOR-like configuration with a major radius $R = 1.8$ m, a minor radius $a = 0.45$ m and the safety factor at the boundary $q_a = 3.0$ is employed.

The simulated image (assumed emission profile $E = \exp(-((\rho - 0.9)/0.1)^2) \times \exp(-im\theta)$ and $m = 10$) with noise levels of 6% and 20% are shown in Figs. 4 (C) and (D), respectively. Here, the normally distributed random noise with zero mean and standard deviations of 6% and 20% of the maximum value of I on all channels are shown. The reconstructions by the P-T method are shown in Figs. 4 (E) and (F). Reasonable reconstructed profiles are obtained when the line-integrated image is significantly disturbed with 20% noise. The minimal values of d^2 for the two noise levels (6% and 20%) are 0.007 and 0.02, respectively (which is 0.0004 for the case without any added noise).

The reconstructions for emissions with higher mode numbers are also investigated. An example of a test with

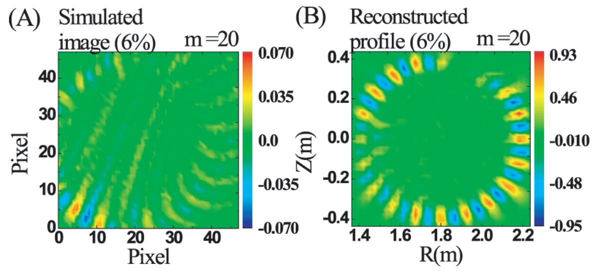

Fig. 5 Tests with m = 20 in the tokamak configuration: the simulated image with 6% added noise (A) and the profile (B) reconstructed from (A).

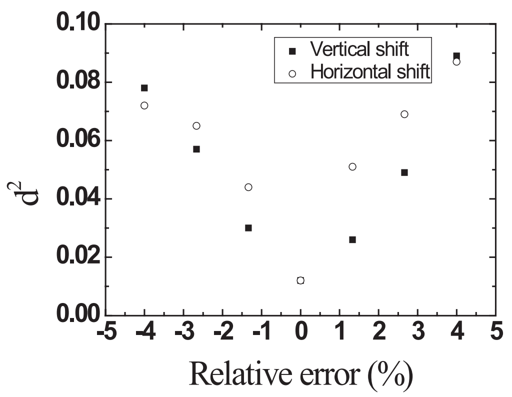

Fig. 6 Variations in the residual deviation resulting from the accuracy of the placement of the diagnostics.

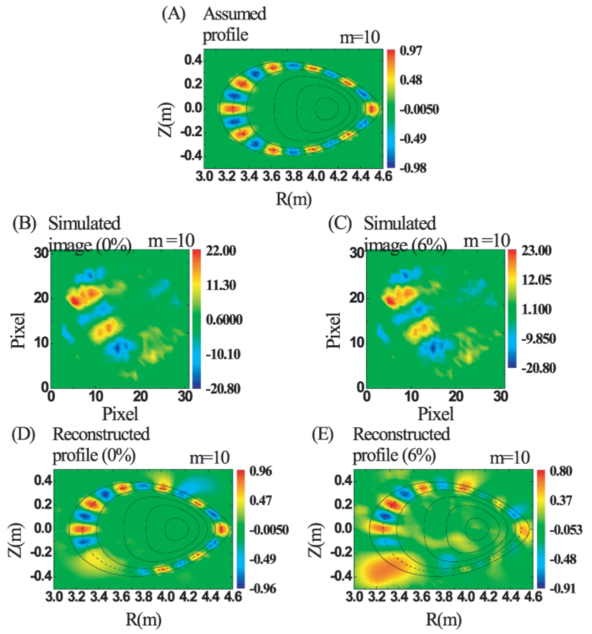

Fig. 7 Assumed profile (A), simulated images with 0% noise (B) and 6% added noise (C), and reconstructed profiles (D), (E) from (B) and (C), respectively, with a LHD configuration.

m = 20 is shown in Fig. 5; Figure 5 (A) is the simulated image with 6% added noise and (B) is the profile reconstructed from (A), where the minimal d^2 is about 0.008. The numerical tests show that the fluctuations can be resolved even at higher mode numbers (e.g., m =20); this is the major advantage of the tangentially viewing lines [10].

In this configuration, the effect on reconstructions from the accuracy of the placement of the diagnostics is investigated by adjusting the detector horizontally and vertically. The minimal value of d^2 becomes eight times larger in the case of a 4% shift from the original position (Fig. 6). The horizontal axis indicates the relative shift error. The negative values correspond to a leftward (downward) shift in the horizontal (vertical) direction.

4.2 Numerical tests with LHD configuration

The reconstructions by the P-T method have been examined in the more complex LHD configuration. The simulated images, without any added noise [Fig. 7 (B)] and with 6% added noise [Fig. 7 (C)], of the assumed emission profile, which assumes the same form as in the tokamak configuration (mode number m = 10), and the corresponding reconstructed profiles are shown in Figs. 7 (D) and (E). The tests are conducted using the LHD configuration of $<\beta> \sim 1.4\%$ and R_{ax} = 3.75 m. The coverage of the viewing lines is shown in Fig. 2. Reconstructions with a minimal residual deviation d^2 of about 0.02 and 0.05 are obtained. The relatively higher residual deviations is due to the lack of coverage of viewing lines as shown in the lower left region in Figs. 7 (D) and (E).

To investigate the effect of the accuracy of the equilibrium on the reconstructions, an image is simulated using the matrix obtained by the configuration of R_{ax} = 3.75 m, $<\beta> \sim 1.4\%$, and no added noise. Furthermore, three geometry matrices are calculated using three different configurations with the same R_{ax} (R_{ax} = 3.75 m) but different $<\beta>$: ~ 1.0%, 1.4%, and 2.0%. Reconstructions for the same simulated image are attempted using these three geometry matrices and the residual deviations d^2 for the corresponding reconstructed profiles with the optimized regularization parameters are 0.11, 0.02, and 0.14. Therefore, to minimize the residual deviation, the accuracy of the magnetic configuration should be carefully controlled.

5. Summary and Future Work

A tomographic reconstruction technique for tangentially viewing 2D camera system is investigated. A method for calculating the geometry matrix in a 2D tangentially viewing system is introduced. Numerical test results show that the P-T method is suitable for the tomographic reconstruction in both tokamak and LHD configurations. We can reconstruct the mode structure with a relatively high poloidal mode number (~ m = 20) in phantom simulations. The calculation of the geometry matrix demands high accuracy and strongly depends on the magnetic configurations. Reconstructions with experimental data using the algorithm based on a P-T type regularization method will be performed in a future study.

Acknowledgments

The authors thank Prof. N. Iwama and the technicians involved in the LHD experiment for their useful advice and support. This work is supported by the NIFS budget code ULPP021, the IAEA TEXTOR agreement (NIFS budget code KETE001), and is partially supported by the JSPS-CAS Core-University program in the field of "Plasma and Nuclear Fusion."

[1] S. Ohdachi, K. Toi and LHD Experimental Group, G. Fuchs, S. von Goeler and S. Yamamoto, Rev. Sci. Instrum. **74**, 2136 (2003).
[2] D.G. Nilson, M.E. Fenstermacher, R. Ellis, G. Brewis, N. Jalufka and R.T. Snider, Rev. Sci. Instrum. **70**, 738 (1999).
[3] M. Takeuchi, S. Ohdachi and LHD experimental group, Plasma Fusion Res. **5**, S1037 (2010).
[4] N. Iwama, H. Yoshida, H. Takimoto, Y. Shen, S. Takamura and T. Tsukishima, Appl. Phys. Lett. **54**, 502 (1989).
[5] G.H. Golub, M. Heath and G. Wahaba, Technometrics **21**, 215 (1979).
[6] L.C. Ingesson, B. Alper, B. J. Peterson and J.-C. Vallet, Fusion Sci. Technol. **53**, 528 (2008).
[7] S. Ohdachi *et.al.*, Plasma Sci. Technol. **8**, 45 (2006).
[8] Y. Suzuki *et al.*, Nucl. Fusion **46**, L19 (2006).
[9] Y. Suzuki *et al.*, Contrib. Plasma **50**, 576 (2010).
[10] S. von Goeler *et al.*, Rev. Sci. Instrum. **61**, 2055 (1990).